

# A Computational Fluid Dynamics (CFD) Analysis of an Undulatory Mechanical Fin Driven by Shape Memory Alloy

Yong-Hua Zhang\*, Jian-Hui He, Jie Yang, Shi-Wu Zhang

Department of Precision Machinery and Precision Instrumentation,  
University of Science and Technology of China, Hefei 230027, PRC

Kin Huat Low

School of Mechanical and Aerospace Engineering, Nanyang Technological University, 50 Nanyang Avenue, Singapore 639798,  
Republic of Singapore

---

**Abstract:** Many fishes use undulatory fin to propel themselves in the underwater environment. These locomotor mechanisms have a popular interest to many researchers. In the present study, we perform a three-dimensional unsteady computation of an undulatory mechanical fin that is driven by Shape Memory Alloy (SMA). The objective of the computation is to investigate the fluid dynamics of force production associated with the undulatory mechanical fin. An unstructured, grid-based, unsteady Navier-Stokes solver with automatic adaptive remeshing is used to compute the unsteady flow around the fin through five complete cycles. The pressure distribution on fin surface is computed and integrated to provide fin forces which are decomposed into lift and thrust. The velocity field is also computed throughout the swimming cycle. Finally, a comparison is conducted to reveal the dynamics of force generation according to the kinematic parameters of the undulatory fin (amplitude, frequency and wavelength).

**Keywords:** Computational Fluid Dynamics (CFD), undulatory mechanical fin, unsteady flow, unstructured mesh, Shape Memory Alloy (SMA).

---

## 1 Introduction

There are various kinds of fishes living in the underwater environment possessing daedal swimming mode which can be divided into two types based on the propulsive structure used: body and/or caudal fin locomotion (BCF) and median and/or paired fin locomotion (MPF)<sup>[1]</sup>. Swimming performance shows that fin based propulsors in some fishes are capable of generating thrusts that can power a very high speed<sup>[2]</sup>. In addition, these fishes are highly maneuverable in a complex three-dimensional underwater environment. For example, Batoids propel themselves through the water with their greatly expanded pectoral fins to achieve agile movement<sup>[3]</sup>.

Nowadays, many new concepts of biologically-inspired design have been developed<sup>[4]</sup>. Several biomimetic fish-like underwater robots have been built with fins<sup>[5,6]</sup>, whereas others use smart material, such as Ionic Conducting Polymer gel Film (ICPF) to mimic the soft fin locomotion<sup>[7,8]</sup>. However, no detailed fluid

mechanisms of these unsteady mechanical fin motions were shown. The work presented in this paper is particularly important for the mechanical design as well as for evaluating power consumption.

Computational Fluid Dynamics (CFD) simulations can solve the Navier-Stokes equations, which account for all fluid mechanical effects. However, the application of CFD to the case of an undulatory fin can be tedious due to the large computational resources required to simulate the moving boundary of the fin. Liu and Kawachi<sup>[9,10]</sup> used the CFD method to simulate 2D and 3D dimensional hydrodynamics of Tadpole locomotion. Other researchers published results of three-dimensional unsteady computations of pectoral fin<sup>[11,12]</sup>.

In this study, an undulatory mechanical fin driven by Shape Memory Alloy (SMA) is developed, and the flow field around the mechanical fin with two undulating sides is computed by CFD technique. The pressure distribution on fin surface is computed and integrated to give fin forces, which are decomposed into lift and thrust. The velocity field is also computed throughout the swimming cycle. The feature of flow field and hydrodynamic forces acting on the fin is discussed based

---

Manuscript received July 11, 2006; revised August 28, 2006.

\*Corresponding author. *E-mail address:* yhzhang@ustc.edu

on the computed results. Finally, a comparison is conducted to reveal the dynamics of force generation according to the kinematic parameters of the undulatory fin (amplitude, frequency and wavelength). These results may help to understand the complex fluid mechanics of the mechanical fin, which is used to generate thrust.

The objectives of this study are as follows:

- 1) To build an accurate three-dimensional CFD model of an undulatory swimming mechanical fin ( $Re = 2000$ )
- 2) To quantify the thrust and drag forces acting on the fin
- 3) To demonstrate the influence of kinematic parameters change on force generation
- 4) To show the influence of undulatory fin motion on the boundary layer.

The remaining of this paper is organized as follows: In Section 2, we discuss the principle of mechanical design of the undulatory bionic fish fin. Section 3 presents the CFD model, including unstructured mesh generation, adaptive re-meshing, kinematic model, forces and power calculations. In Section 4, several experimental results are presented and analyzed in detail, and conclusion and future work are given in Section 5.

## 2 Mechanism design of undulatory fin

### 2.1 Mechanism structure

We use SMA as an actuator to create the robotic fin which is shown in Fig. 1. In the preliminary trials, the robotic fin is designed to have a dimension of 50 mm×40 mm×1 mm. This small fin dimension is chosen for several reasons. The most important one is that we would like to consider the feasibility to build a micro underwater propulsion system using SMA. The

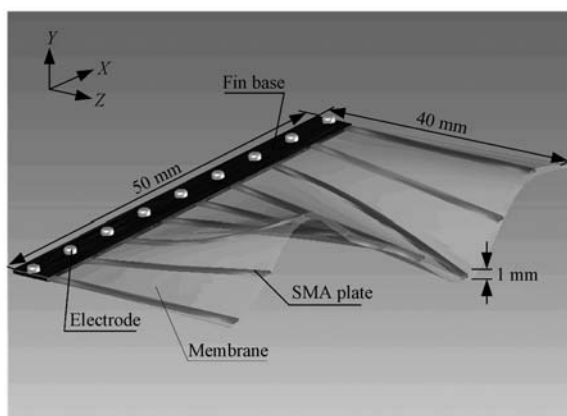


Fig. 1 Generation of oscillatory and undulating fin motions

fin consists of three main parts: nine couples of SMA plates, elastomer sheet and fin base. The nine couples of SMA plates work as the function of fin-ray, which can form any fin shape when specially arranged. Thin elastomer sheet is in fact an ideal material, which can be used to model a flexible membrane. In this application, however, the rubber is required to elongate more than 150% of its initial length, and extra power is therefore needed in addition to the power required to push water. The fin base is used to fix the SMA plates. This bionic fin can realize different locomotion modes by different heating scheduling. In this paper only undulatory motion of the fin is under discussion. Refer to [13] for the details about the fin structure.

### 2.2 Kinematic model

Although the working process of our SMA driven robotic fin is discrete, the fin movements for the undulatory swimming can still be expressed as sinusoidal with the amplitude gradually increasing along with  $x$  and  $z$  axes if there are enough couples of SMA plates. The method greatly simplifies the imitation calculation. We also suppose the linear change of amplitude along the two axes with slope  $k = 1$  for simplification. The undulatory equation can then be described as follows:

$$y(x, z, t) = A(x, z) \sin \left[ 2\pi \left( \frac{x}{\lambda} - \frac{t}{T} \right) \right] \quad (1)$$

$$A(x, z) = kxz \quad (2)$$

where  $A(x, z)$  represents the wave amplitude related to  $x$  and  $z$  variables,  $t$  is the time step,  $\lambda$  is the wavelength, and  $T$  is the period of undulatory. In our case study, we assume that  $\lambda = 25$  mm and  $T = 0.25$  s.

### 2.3 Drag, lift and moment calculations

In order to conduct general comparison, we define the lift ( $C_L$ ), the drag ( $C_D$ ) and the  $x$  axis moment ( $C_M$ ) in non-dimensionalized forms as

$$C_L = \frac{Lift}{2\rho U^2 S_{fin}} \quad (3)$$

$$C_D = \frac{Drag}{2\rho U^2 S_{fin}} \quad (4)$$

$$C_M = \frac{Trust \times d}{2\rho U^2 S_{fin}} \quad (5)$$

where  $S_{fin}$  is the fin surface area, and  $d$  is the distance between force vector and  $x$  axis. (see Fig. 2 for more details).

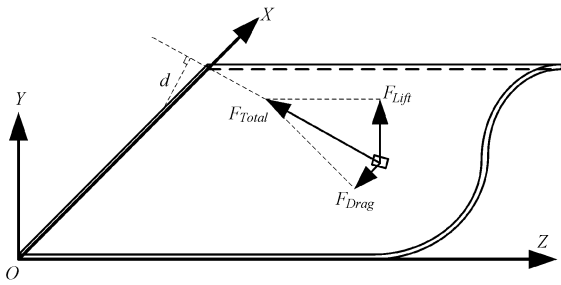


Fig. 2 Coordinate system

### 3 Materials and methods

#### 3.1 Model of CFD

The governing equations are the incompressible, unsteady Navier-Stokes given by

$$\begin{cases} \frac{\partial u}{\partial t} + u \frac{\partial u}{\partial x} + v \frac{\partial u}{\partial y} + w \frac{\partial u}{\partial z} = -\frac{1}{\rho} \frac{\partial p}{\partial x} + \nu \left( \frac{\partial^2 u}{\partial x^2} + \frac{\partial^2 u}{\partial y^2} + \frac{\partial^2 u}{\partial z^2} \right) \\ \frac{\partial v}{\partial t} + u \frac{\partial v}{\partial x} + v \frac{\partial v}{\partial y} + w \frac{\partial v}{\partial z} = -\frac{1}{\rho} \frac{\partial p}{\partial y} + \nu \left( \frac{\partial^2 v}{\partial x^2} + \frac{\partial^2 v}{\partial y^2} + \frac{\partial^2 v}{\partial z^2} \right) \\ \frac{\partial w}{\partial t} + u \frac{\partial w}{\partial x} + v \frac{\partial w}{\partial y} + w \frac{\partial w}{\partial z} = -\frac{1}{\rho} \frac{\partial p}{\partial z} + \nu \left( \frac{\partial^2 w}{\partial x^2} + \frac{\partial^2 w}{\partial y^2} + \frac{\partial^2 w}{\partial z^2} \right) \end{cases} \quad (6)$$

with the continuity equation

$$\frac{\partial u}{\partial x} + \frac{\partial v}{\partial y} + \frac{\partial w}{\partial z} = 0 \quad (7)$$

where  $x, y$  and  $z$  are the axes of the orthogonal coordinate system, while  $u, v$  and  $w$  are the fluid velocity vectors in each direction respectively,  $p$  is the pressure, and  $\rho$  the fluid density. Turbulence quantities are not considered in the governing equations because the laminar flow is assumed for this computation in our study. All the fluid variables are made dimensionless with respect to the uniform inflow  $U$ , the length of the fin  $L$ , and the fluid density  $\rho$  respectively. The dimensionless parameter of the Reynolds number ( $Re$ ) is defined as

$$Re = UL/\nu \quad (8)$$

where  $\nu$  is the kinematic viscosity, with a value of  $1.533 \times 10^{-6} \text{ m}^2/\text{s}$ . Given a body length of 50 mm in our model and a reasonable and realistic forward swimming speed of 60 mm/s, we calculate an  $Re$  of about 2000. The governing equations are discretized using the finite volume method (FVM) with an implicit segregated solver approach. The Navier-Stokes momentum equations are discretized with a second order upwind scheme, while pressure is interpolated using a second order accurate scheme. An implicit first order scheme is used for temporal discretization, with a time step size of 0.002 seconds. Simulations are carried out for 500 time steps to simulate swimming for more than four tailbeat periods. Pressure velocity coupling of the

continuity equation is achieved using the SIMPLE algorithm that is valid for the small time steps used in the simulation.

#### 3.2 Unstructured mesh generation and adaptive re-meshing

If the bodies move through the flow field, the positions of relevant flow features will change. Therefore, in most of the computational domain, a new mesh distribution is required. One approach to solving these problems is to add a moving grid system. Accordingly, we make the grids fit the deforming boundaries at each physical time step, and also make sure that there is sufficient grid density to resolve the viscous and unsteady flows both around the body surface and in the wake. As the elements (or edges) move, their geometric parameters (shape-function derivatives, *etc.*) need to be recomputed at each time step. If the whole mesh is assumed to be in motion, then these geometric parameters need to be recomputed globally. In order to reduce the number of global remeshings and computation load, only a small number of elements surrounding the bodies are assumed to be in motion. The remainder of the field is then treated in the usual Eulerian frame of reference, avoiding recomputing geometric parameters. In developing boundary conditions on the body surface, a no-slip condition is used for the velocity components, which is to say that the velocity of a fluid particle is equal to the velocity of the swimmer at that point. Details of the algorithm can be found in the work by Ramamurti *et al.*<sup>[11]</sup>. The exact geometry and the corresponding surface mesh of the undulatory mechanical fin are shown in Fig. 3. The computational mesh consists of 150 026 nodes and 840 379 tetrahedral elements, which are sufficient for resolving the inviscid flow through this configuration. The boundary condition for the inlet is steady uniform flow at 0.06 m/s. The downstream boundary is modeled as a constant pressure outlet, while the sides are modeled as no-slip walls. Both of the fin surfaces are simulated as a smooth no-slip wall.

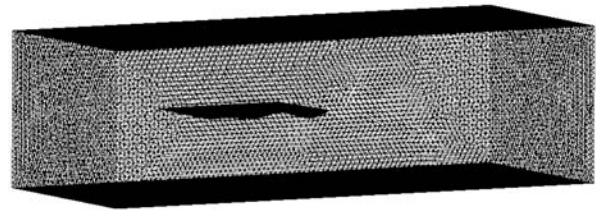


Fig. 3 Computational meshes for undulatory mechanical fin

All the computations were carried out on a PC with a P4 2.8 CPU and 2G memory. Data were autosaved in harddisk for further processing. The computation took two days for each case.

## 4 Results and discussion

### 4.1 Pressure distribution

The computations were carried out using the prescribed fin kinematics with swimming at  $U = 60$  mm/s. The maximal amplitude is approximately 8 mm, the frequency of fin undulatory is 4 Hz and the wavelength is 25 mm, resulting in a mean traveling wave speed of  $C = 100$  mm/s approximately. Therefore, the ratio of wave speed to swimming velocity is  $C/U = 5/3$ . The three and two-dimension pressure contours at  $t = 0.01$  s of the fourth period are shown in Figs. 4 and 5, respectively. Fig. 4 shows three-dimension pressure contours of the mechanical fin in the simulation. Since the wave amplitude is gradually increased along direction from the leading edge (left) to the trailing edge (right), so does the pressure. As can be seen from Fig. 4, the pressure is quite small at the leading edge area and reaches its maximum at the trailing edge area. The pressure difference between the upper surface and the lower surface is the cause of thrust and drag production. We can also see that the pressure is gradually increased along the direction from fin base to fin tip in Fig. 5. It's in some parts because of the increment of undulatory amplitude too.

We use four slices at different  $z$  locations ( $z = 5$  mm, 15 mm, 25 mm, 35 mm) at the  $t = 0.01$  s of the fourth period to give a clear description of the pressure distribution along  $z$  direction. The pressure changes

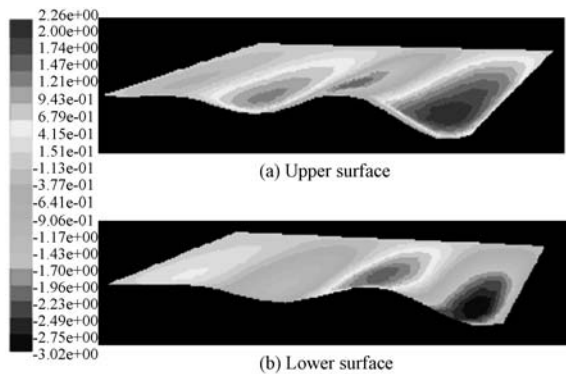


Fig. 4 Three-dimension pressure contours of the mechanical fin surface: (a) The upper surface; (b) The lower surface

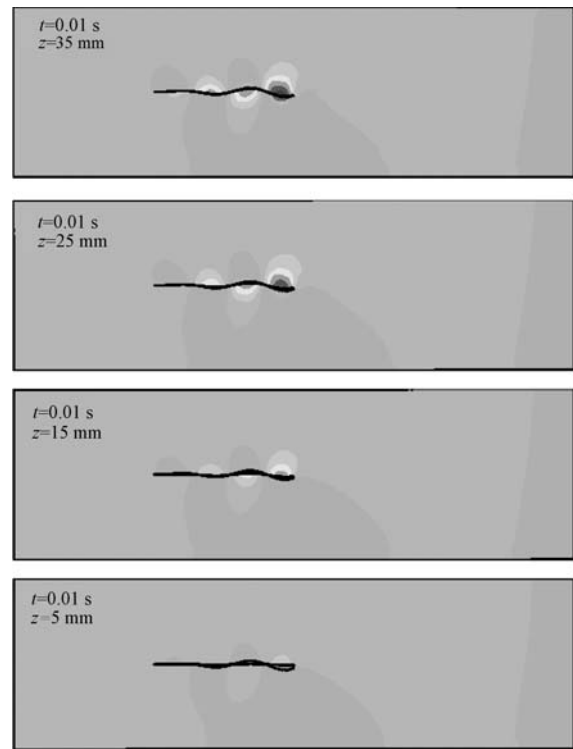


Fig. 5 Slices with different coordinates along  $z$  axis at  $t = 0.01$  s

dramatically along with  $z$  coordinate variety. At  $z = 35$  mm, the pressure on fin surface is much larger than that at  $z = 5$  mm location.

In order to provide detailed information on the flow about the fin during periodical motion, we examined the surface pressure contours. Fig. 6 shows the surface pressure contours in  $\text{N/m}^2$ , on the undulatory mechanical fin at four instants (At  $t = 0T$ , the beginning of cycle  $T$ ,  $t = 0.32T$ , 32% of the cycle,  $t = 0.64T$ , 64% of the cycle, and  $t = 0.96T$ , almost the end of one cycle, respectively). A high pressure region appears at posterior half of the fin length, just as that in Fig. 4, which provides a maximum thrust to propel the mechanism.

### 4.2 Velocity field distribution

Fig. 7 shows the flow velocity vectors on the undulatory mechanical fin at four instants ( $t = 0T$ , at the beginning of cycle,  $t = 0.32T$ , at 32% of the cycle  $T$ ,  $t = 0.64T$ , at 64% of the cycle and  $t = 0.96T$ , almost at the end of one cycle). Streamwise velocity (m/s) contours show the high-velocity jet produced by the fish. With the freestream velocity equal to 0.06 m/s, it can be noted that the high-velocity region is very close to the posterior region of undulatory fin. The wave speed ( $c$ ) for the undulatory fin wave is 0.1 m/s, so the undulatory wave is traveling faster than the swimming wave with a  $C/U$  ratio of 1.67. This allows the crest of the

wave to transform a region of fluid just downstream into a high-velocity jet, which is then carried to the wake.

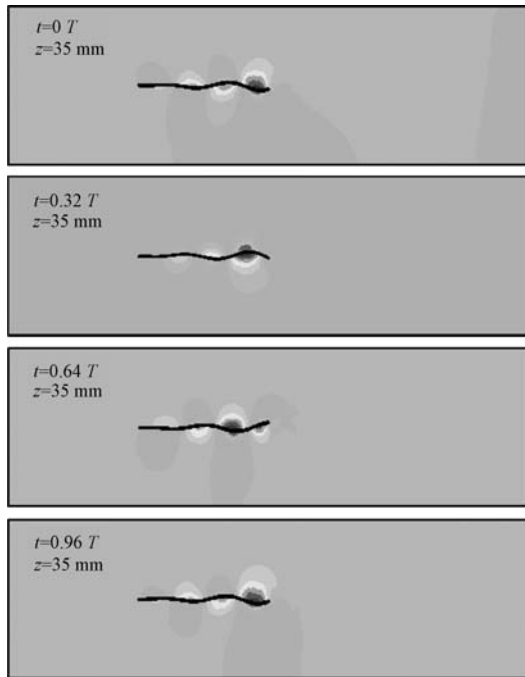


Fig. 6 Pressure contours at  $z = 35$  mm slice during the fourth period

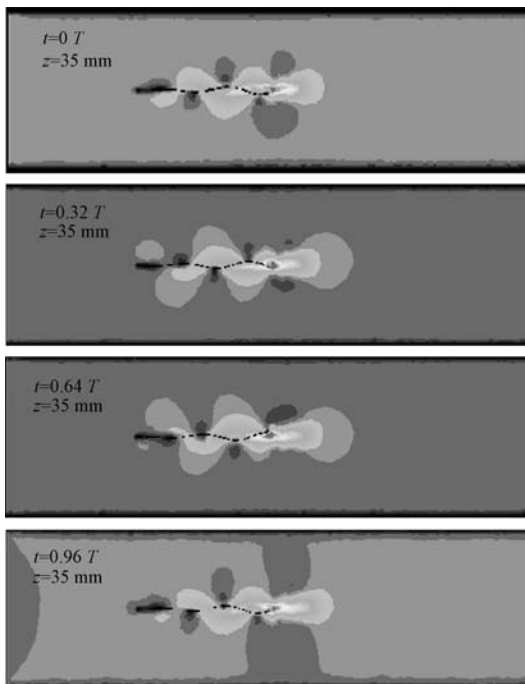


Fig. 7 Velocity vectors on the surface of the mechanical fin at four instants during the fin undulatory at the fourth period. The inlet velocity is 60 mm/s

### 4.3 Drag, lift and moment

In Fig. 8 the drag, lift and moment coefficients are plotted at the second tailbeat period respectively, where the frequency is equal to 4 Hz, wavelength is 25 mm and amplitude slope  $k = 1$ . The period-averaged nondimensional drag coefficient was calculated to be  $-0.00016$ , whereas the period-averaged lift was calculated to be almost zero, This was also happened to  $x$  axis moment, where thrust was equal to drag for steady swimming.

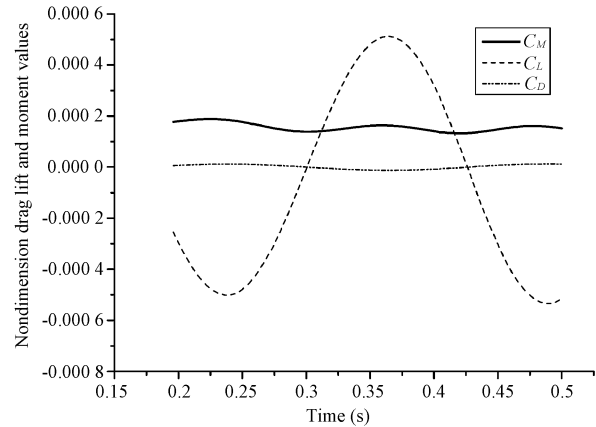


Fig. 8 The variation at the second tailbeat period of the forces acting on the whole fin surface. Drag is equal to thrust for steady swimming

### 4.4 Dynamics of force with respect to kinematic parameters

In this subsection, we will examine the influence of the kinematic parameters. The undulatory frequency, amplitude and wavelength are changed individually. Then the results are presented and analyzed.

Fig. 9 displays the pressure distribution under different frequencies and Fig. 10 delivers the dynamics of thrust with respect to frequency. At the time  $t = 0.96T$  (see Fig. 9), the maximum pressure value is about 2.264 Pa when the frequency = 4 Hz, while 10.164 Pa at frequency = 10 Hz. The generated force on fin surface changes with frequency. As shown in Fig. 10, the maximum period-averaged nondimensional drag coefficient is about  $-0.00024$  at the frequency of 10 Hz, while  $-0.00016$  at 4 Hz. The thrust is 1/3 higher with the increase of swimming frequency.

The undulatory fin wavelength has some influence on swimming efficiency and thrust generation. Fig. 11 shows the pressure contour under different motion wavelengths: (a) 25 mm and (b) 45 mm. Fig. 12 shows the period-averaged nondimensional drag coefficient with respect to wavelength. The maximum pres-

sure value is about 2.264 Pa at wavelength = 25 mm, while 3.474 Pa at wavelength = 45 mm.

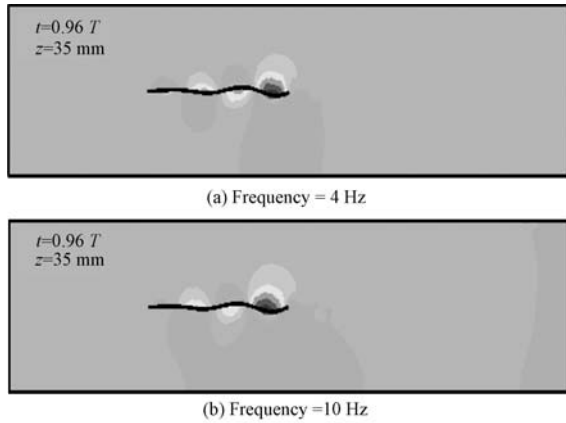


Fig. 9 Pressure distribution under different motion frequencies: (a) Frequency of 4 Hz, (b) Frequency of 10 Hz

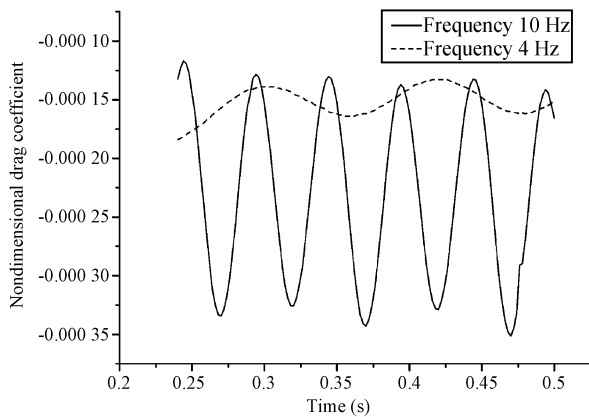


Fig. 10 Thrust changes with frequency

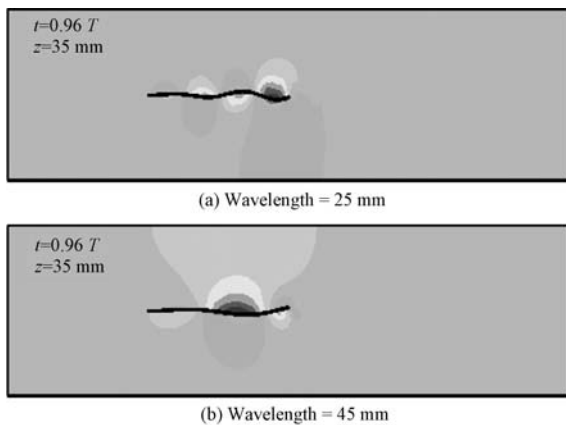


Fig. 11 Pressure distribution under different motion wavelengths: (a) Wavelength of 25 mm, (b) Wavelength of 45 mm

The period-averaged nondimensional drag coefficient is about  $-0.00016$  at wavelength = 25 mm, while

$-0.0026$  at wavelength = 45 mm. The thrust is also increased with the increase of swimming wavelength. This also implies an evidence that anguilliform swimming model (using the whole body to undulate and propel through a short wavelength) has lower swimming efficiency and produces less thrust than other swimmers, who uses longer wavelength for propulsion.

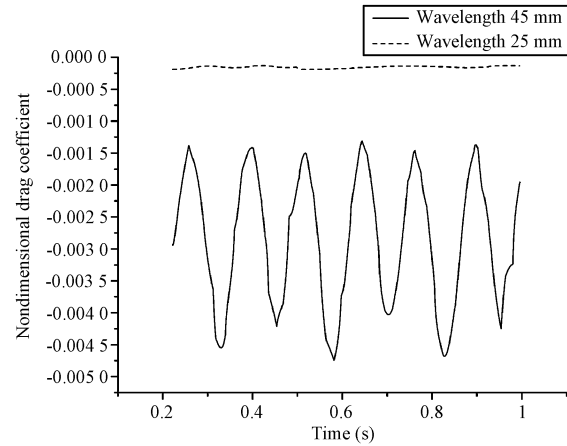


Fig. 12 Thrust changes with wavelength

Fig. 13 displays the pressure distribution under different amplitudes and Fig. 14 delivers the dynamics of thrust with respect to amplitude. Undulatory amplitude is controlled by slope  $k$ . The higher  $k$  provides the larger undulatory amplitude. The maximum pressure value is about 2.264 Pa at  $k = 1$ , while 3.492 Pa when  $k = 1.5$ . The period-averaged nondimensional drag coefficient is about  $-0.00016$  at  $k = 1$ , while  $-0.000185$  at  $k = 1.5$ , which means swimming thrust increases with traveling wave amplitude.

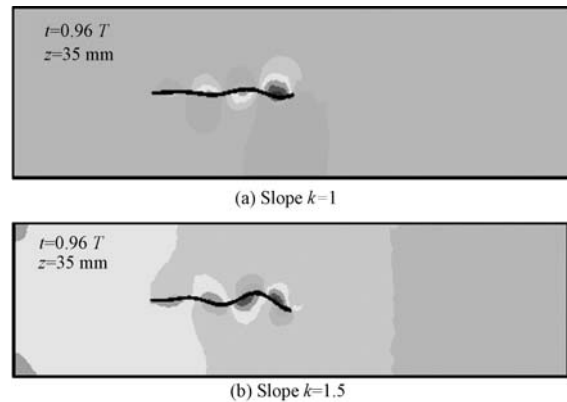


Fig. 13 Pressure distribution under different motion amplitudes: (a) Amplitude slope  $k = 1$ , (b) Amplitude slope  $k = 1.5$

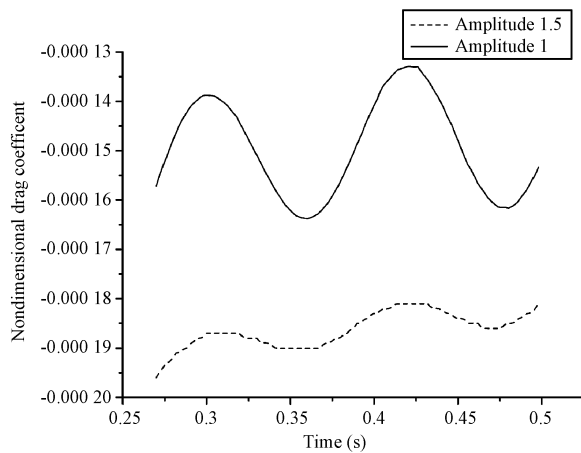


Fig. 14 Thrust changes with amplitude

#### 4.5 Influence of undulatory fin motion on the boundary layer

The undulatory motion is considered to restrain the separation of boundary layer. Here, we use both simulation and experimental results to investigate the statement.

Fig. 15 provides both simulation and experimental results, which show the influence of undulatory fin motion on boundary layer character. When the fin stays still ( $C = 0$  m/s), the boundary layer does separate with a strong vortex detected. When the fin undulates with wave speed  $C = 0.1$  m/s, the separation of boundary layer can be restrained. This phenomena is also mentioned by Yang and Yin<sup>[14]</sup> who presented that the separation is restrained when  $C/U$  ratio is greater than 1. A more detailed study on the effect of  $C/U$  on

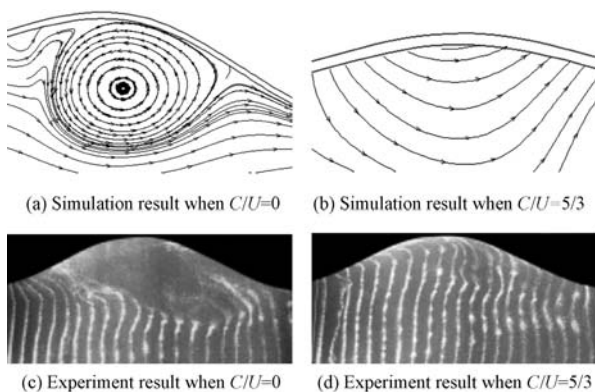


Fig. 15 Both simulation (a), (b) and experiment (c), (d) results to show the influence of undulatory motion on boundary layer character. A strong vortex in the boundary layer is generated when the fin keeps still (see figures (a) and (c)); the vortex disappeared when fin moves in undulatory motion (see figures (b) and (d))

the suppression of separation, drag reduction and power consumption can be found in [15].

## 5 Conclusion and future work

In the present study, an undulatory mechanical fin driven by SMA is developed, and the flow field around the mechanical fin is computed and obtained by CFD technique. We find the pressure and velocity distributions on the fin surface, and evaluate the fin forces, which have been decomposed into lift and thrust. A comparison has been conducted to reveal the dynamics of force generation according to the kinematic parameters of the undulatory fin (amplitude, frequency and wavelength). We conclude that undulatory amplitude, frequency and wavelength have significant effect on thrust generation in certain ranges. Also, the change in wavelength has the strongest influence on thrust generation, because it changes the propulsion model. These results are in accordance with several existing experimental works<sup>[2,6,16]</sup>. Finally, we analyze the undulatory motion influencing fluid character of boundary layer. The boundary layer separation can be well restrained by undulatory fin motion. All of these results are helpful in understanding the complex fluid mechanics of the mechanical fin and deciding the parameters of the fin.

For future work, we should investigate fin swimming mechanisms to better evaluate the model. Fin thickness should be considered in the model, as it might increase drag. Adding turbulence to the three-dimensional simulation would provide the most accurate and realistic numerical simulation of mechanical fin motion.

## References

- [1] J. B. C. Davies, B. Deacon, D. M. Lane, M. Sfakiotakis. Fish Swimming Gaits. [Online], Available: <http://www.ece.eps.hw.ac.uk/Research/oceans/projects/flaps/mp-fmodes.htm>, August, 2006.
- [2] J. A. Walker, M. W. Westneat. Performance Limits of Labriform Propulsion and Correlates with Fin Shape and Motion. *The Journal of Experimental Biology*, vol. 205, no. 2, pp. 177–187, 2002.
- [3] L. J. Rosenberger. Pectoral Fin Locomotion in Batoid Fishes: Undulation Versus Oscillation. *The Journal of Experimental Biology*, vol. 204, no. 22, pp. 379–394, 2001.
- [4] P. R. Bandyopadhyay. Maneuvering Hydrodynamics of Fish and Small Underwater Vehicles. *Integrative and Comparative Biology*, vol. 42, no. 1, pp. 102–117, 2002.
- [5] N. Kato, M. Furushima. Pectoral Fin Model for Maneuver of Underwater Vehicles. In *Proceedings of the 1996 Symposium on Autonomous Underwater Vehicle Technology*. Monterey, CA, pp. 49–56, 1996.
- [6] K. H. Low, A. Willy. Development and Initial Investigation of NTU Robotic Fish with Modular Flexible Fins. In *Proceedings of the IEEE International Conference on Mechatronics & Automation (ICMA2005)*, Niagara Falls, Canada, pp. 958–963, 2005.

- [7] S. Guo, Y. Okuda. Characteristic Evaluation of an Underwater Micro Biped Robot with Multi DOF. In *Proceedings of the 2004 International Conference on Intelligent Mechatronics and Automation*, Chengdu, China, pp. 95–100, 2004.
- [8] S. Guo, Y. Okuda, K. Asaka. A Novel Type of Underwater Micro Biped Robot with Multi DOF. In *Proceedings of the 2004 IEEE International Conference on Robotics and Automation*, Barcelona, Spain, pp. 4881–4886, 2004.
- [9] H. Liu, K. Kawachi. A Numerical Study of Undulatory Swimming. *Journal of Computational Physics*, vol. 155, no. 2, pp. 223–247, 1999.
- [10] H. Liu, K. Kawachi. The Three-dimensional Hydrodynamics of Tadpole Locomotion. *The Journal of Experimental Biology*, vol. 200, no. 4, pp. 2807–2819, 1997.
- [11] R. Ramamurti, W. C. Sandberg, R. Lohner, J. A. Walker, M.W. Westneat. Fluid Dynamics of Flapping Aquatic Flight in the Bird Wrasse: Three-dimensional Unsteady Computations with Fin Deformation. *The Journal of Experimental Biology*, vol. 205, no. 19, pp. 2997–3008, 2002.
- [12] Hiroyoshi Suzuki, Naomi Kato. A Numerical Study on Unsteady Flow Around a Mechanical Pectoral Fin. *International Journal of Offshore and Polar Engineering*, vol. 15, no. 3, pp. 161–167, 2005.
- [13] Y. Zhang, J. He, J. Yang. Design and investigation of shape memory alloy dce on robotics and biomimetics. In *Proceedings of the IEEE International Conference on Robotics and Biomimetics (ROBIO2006)*, Kunming, China, to be published.
- [14] Y. Yang, X. Yin, X. Lu. Flow visualization over a 2D traveling wave wall. *Journal of Experiments in Fluid Mechanics*, vol. 9, no. 2, pp. 84-90, 2005.
- [15] G. J. Dong, X. Y. Lu. Numerical Analysis on the Propulsive Performance and Vortex Shedding of Fish-like Travelling Wavy Plate. *International Journal for Numerical Methods in Fluids*, vol. 48, no. 12, pp. 1351–1373, 2005.
- [16] K. H. Low, A. Willy. Biomimetic motion planning of an undulating robotic fish fin. *Journal of Vibration and Control*, to be published.



**Yong-Hua Zhang** received his B.Sc. degree in precision instrumentation and precision machinery from University of Science and Technology of China, Hefei, China, in 2003. He is now pursuing his Ph.D. degree in University of Science and Technology of China.

He has published over 10 refereed journal and conference papers. His current research is about biomimetic robotic fish fin using smart material (SMA). His research interest also includes underwater microrobots utilizing artificial muscles.



**Jian-Hui He** received her B.Sc. degree in computer science from China Agriculture University, Beijing, China, in 2003. She is now pursuing her M.Sc degree in Department of Precision Machinery and Precision Instrumentation, University of Science and Technology of China. Currently, she is working on the influence of electric field's strength on the fabrication of micro droplet lens.

She has published 5 refereed journal and conference papers in recent two years. Her research interests include micro-optics and underwater robots.



**Jie Yang** graduated from the Department of Physical Chemistry at the Beijing University of Science and Technology, in 1969. He is currently a professor in the Department of Precision Machinery and Precision Instrumentation of University of Science and Technology of China. He leads several research groups focusing on intelligent robots supported by the National Natural Science Foundation of China and 863 Project.

His research interests include intelligent robots, precision machinery materials, and high speed photography.



**Shi-Wu Zhang** received his B.Sc. degree in mechanical and electrical engineering and the Ph.D. degree in precision instrumentation and precision machinery from University of Science and Technology of China, Hefei, China. He is currently a research assistant in the Department of Precision Machinery and Precision Instrumentation, University of Science and Technology of China. He has been a research assistant in the Department of Computer Science, Hong Kong Baptist University for one and a half years.

His current interests include web intelligence, autonomy oriented computation, complex systems, and intelligent robots.



**Kin Huat Low** received his M.Sc and Ph.D. degrees in mechanical engineering from the University of Waterloo, Canada, in 1983 and 1986, respectively. After spending two years as a post-doctoral fellow at the University of Waterloo, he joined the School of Mechanical and Aerospace Engineering of the Nanyang Technological University.

He is the author of five books and more than 90 journal papers in the areas of biomimetics, robotics, rehabilitation, impacts, power transmission systems, structural dynamics and vibrations. His research interests include robotics, vibrations, impacts, machines, mechanisms, exoskeleton systems, and mechatronics design.

Dr. Low is a member of IEEE, IASTED, SIAA and SiC-ToMM. He is also a member of several technical, conference committees, and journal editorial boards. He has won awards at the two IEEE conferences on the research work on robotics fish and powered exoskeleton, respectively.